Research on Chemical Intermediates (2022) 48:1847–1861
https://doi.org/10.1007/s11164-022-04704-x

A bis(rhodamine 6G)-based fluorescent sensor for Hg^{2+}: microwave-assisted synthesis, photophysical properties, and computational studies

Oyedoyin Aduroja[1] · Roosevelt Shaw[1] · Fasil Abebe[1]

Received: 13 October 2021 / Accepted: 11 March 2022 / Published online: 22 March 2022

Abstract

A fluorescent and colorimetric sensor based on rhodamine 6 g (**RD6g**) was designed, synthesized, and characterized using microwave irradiation. The sensing behavior of this compound was studied by UV–visible and fluorescence spectroscopy. Sensor **RD6g** exhibits a high selectivity and an excellent sensitivity and is a dual-responsive colorimetric and fluorescent Hg^{2+}-specific sensor in aqueous buffer solution. Mercury ions give rise to the development of a very fluorescent ring-open amide spirolactam system. The detection limit for Hg^{2+} was found to be 1.2×10^{-8} M. The binding ratio of RD6g-Hg^{2+} complex was determined to be 1:1 according to the Job's plot. The reversibility of RD6g·Hg^{2+} complex has been achieved with CN^- anions. The test strip based on **RD6g** was developed, which could be used as a suitable and methodical Hg^{2+} test kit.

Keywords Microwave synthesis · Fluorescent sensor · Rhodamine · Hg^{2+} ions

Introduction

Mercury, one of the most prevalent toxic metals in the environment, easily passes through biological membranes such as skin, respiratory, and gastrointestinal tissues [1]. It plays a role in the food cycle, just as it exists in certain fish [2]. Even at low concentrations, Hg^{2+} can cause great harm to human function. It can be deposited in various forms in the brain, liver, kidneys, and digestive system and causes other inflammations even death [3–6]. Mercury was listed as one of the priority pollutants according to the U.S. EPA [7]. Due to the severe toxicity to human neurological and environmental systems, helpful methods for the detection of Hg^{2+} are urgently demanded. There are a lot of traditional detection methods for Hg^{2+}, including gas

✉ Fasil Abebe
Fasil.Abebe@morgan.edu

[1] Department of Chemistry, Morgan State University, Baltimore, MD 21251, USA

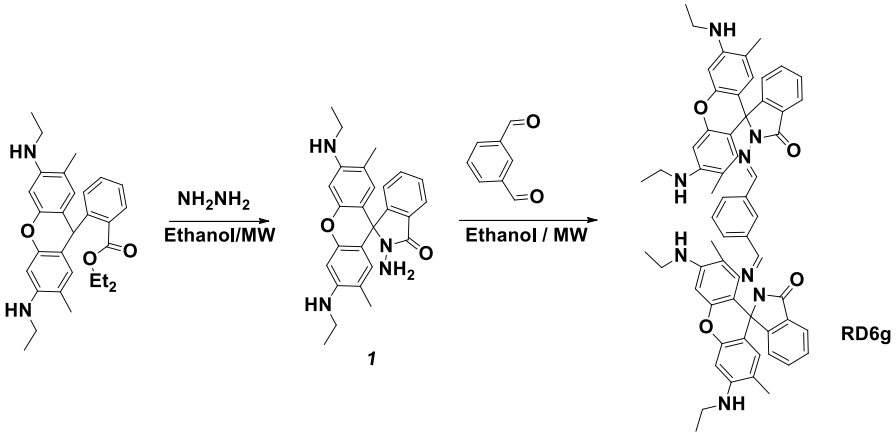

Scheme 1 Synthesis of sensor **RD6g**

chromatography [8], inductively coupled plasma mass spectrometry (ICP-MS) [9], electrochemical method [10], and atomic absorption spectrometry [11]. However, most of them require tedious sample preparation and complex instrumentation, which limits their practical applications. Fluorescence sensing of Hg^{2+} has received considerable attention due to the fast response, 'naked-eye' detection, low cost, excellent sensitivity, selectivity, and other advantages.

Rhodamine-based compounds have been widely used as chemosensors due to their remarkable spectroscopic properties including high absorption coefficients, high fluorescent quantum yields, and excitation and emission with the visible wavelength region [12]. Under these fascinating properties, various rhodamine-based chemosensors have been widely used for the recognition of the numerous analytes. Rhodamine derivatives are non-fluorescent and colorless, but ring-opening of the corresponding spirolactam produces strong fluorescence emission and pink color [12–14]. This property provides an ideal model for constructing OFF–ON fluorescent sensors. The cation-sensing mechanism of most of the rhodamine probes is based on a change from the spirolactam to an open-ring amide, resulting in a color change, highly fluorescent compound [15–20]. Thus, most of the sensors comprise of rhodamine core structure, especially for Hg^{2+} metal ion-based sensors, are of chromogenic and fluorogenic types [16]. There have been many reports of Hg^{2+} ion probes in recent years [21–26]. However, since Hg^{2+} ions are generally used as quenchers due to the spin–orbit coupling effects, most of the probes have problems such as high detection limit [27], poor water solubility [28], and toxicity of sulfur [29]. Therefore, designing dual-channel probes with naked eye recognition and turn-on fluorescent signals in an aqueous solution has attracted more attention.

Here, we report a new rhodamine-based receptor (**RD6g**), substituted with phenyl ring on both sides are synthesized (Scheme 1) as a turn-on fluorescent sensor for Hg^{2+} detection. The rhodamine moiety is incorporated on both the side of the phenyl ring to enhance the chelation sites for Hg^{2+} and achieve a lower detection limit. The synthesized sensor **RD6g** demonstrates extremely selective and sensitive fluorescent

enhancement after the addition of the Hg^{2+} because of the chelation enhanced fluorescence phenomenon. In this paper, a suitable, very clean, and simple microwave-assisted synthesis technique is presented to prepare a rhodamine-based sensor. The coordination of the sensor **RD6g** with Hg^{2+} ion was rigorously investigated by optical spectroscopy, NMR, IR, high-resolution mass spectral analysis (HRMS), and time-dependent density functional theory (TD-DFT) calculations.

Experimental

Materials and instrumentation

All the reagents and solvents were acquired from Sigma-Aldrich including rhodamine 6 g, hydrazine, isophthalaldehyde, ethanol, acetonitrile, and used without further purification. Microwave-assisted reactions were carried out in a CEM microwave reactor. All absorption and fluorescence spectra were recorded using Agilent Cary 60 UV/Vis's spectrometer and Cary Eclipse fluorescence spectrophotometer, respectively. ^{1}H-NMR and ^{13}C-NMR spectra were recorded using Bruker 400 MHz spectrometer. For NMR spectra DMSO-d_6 was used as a solvent using TMS as an internal standard. High-resolution mass spectrometry (HR-MS) was recorded using Bruker 12 T solaris FT-ICR-MS. The IR spectrum was obtained using the Shimadzu IRAffinity FTIR spectrometer. All the measurements were achieved at room temperature.

Preparation of stock solution

The solutions of metal ions were prepared using nitrates [$Co(NO_3)_2$, $Zn(NO_3)_2$, $Ni(NO_3)_2$, $Pb(NO_3)_2$, $Cd(NO_3)_2$, $Hg(NO_3)_2$, $NaNO_3$, KNO_3] or chlorides [$CuCl_2$, $FeCl_3$, $FeCl_2$, $CaCl_2$], and anion species from their tetrabutylammonium salts. All the solutions were prepared in water. Stock solutions of receptor **RD6g** (1×10^{-3} M), selected salts of cations (1×10^{-3} M), and anions (1×10^{-4} M) were prepared in CH_3CN/H_2O. Mercury (II) complex solution ([RD6g·Hg^{2+}]) was prepared by addition of 1.0 equivalent of Hg^{2+} to the solution of **RD6g** (20 μM) in Tris–HCl (10 mM, pH = 7.0) buffer containing acetonitrile/water (9:1 v/v) solution. A simple equation ($DL = 3\sigma/S$) is used for the determination of detection limit (DL) of **RD6g** for Hg^{2+}, where σ is the standard deviation and S is the slope. The association constant between mercury (II) and **RD6g** was estimated from absorption titration data. This was calculated from the Hildebrand equation:

$(1/A - A_0 = 1/K(A_{max} - A_0)[M^{x+}]^n + (A_{max} - A_0))$ Where A_0 is the absorbance of sensors **RD6g** without Hg^{2+}, A is the absorbance of **RD6g** with Hg^{2+} and A_{max} is the absorbance with $[Hg^{2+}]^n{}_{max}$.

DFT studies

Time-density functional theory (TD-DFT) calculations were employed to elucidate the Hg^{2+} interactions with **RD6g** systems. All computations were carried out using

Spartan'18 software package. Geometry optimization of the ground state structures was carried out with TD-DFT at the B3LYP level of theory using 6-31G (d, p) basis set in the gas phase and in both simulated CH_3CN and water media, using a conductor-like polarizable continuum model (CPCM).

Microwave-assisted synthesis of RD6g

Synthesis of **1**: The starting material hydrazide has been prepared according to literature reports [30]. Synthesis of **RD6g**: A mixture of intermediate **1** (100 mg, 0.219 mmol), isophthalaldehyde (16 mg, 0.219 mmol), and ethanol (2 mL) was placed and stirred in a 10 mL reaction vial, and it was placed in the cavity of a CEM microwave reactor. The closed reaction vessel irradiated according to the parameters described in Table S1. The mixture was allowed to cool to room temperature. The solid was filtered, washed with cold ethanol, and air-dried (80% yield). ^{1}H-NMR (DMSO-d_6), δ (ppm): 8.37 (2H, s), 7.92 (2H, d), 7.59 (4H, m, H-Ar), 7.32 (4H, m, H-Ar), 7.03 (2H, d), 6.35 (4H, s), 6.15 (4H, s), 5.07 (4H, m), 3.16 (8H, q, NCH_2CH_3), 1.81 (12H, s, -CH_3), 1.22 (12H, t, NCH_2CH_3). ^{13}C NMR ((DMSO-d_6), δ (ppm): 165.25, 163.95, 151.63, 150.83, 147.36, 144.66, 136.52, 135.37, 134.95, 131.90, 130.77, 129.78, 128.14, 127.32, 126.67, 124.78, 123.72, 122.14, 118.31, 117.79, 104.98, 95.87, 65.27, 37.49, 17.04, 14.20. HRMS (MALDI): m/z Calcd for $C_{60}H_{58}N_8O_4$: 955.15; Found: 955.47.

Results and discussion

Microwave-assisted synthesis and design of RD6g

The target sensor **RD6g** was synthesized using a microwave-assisted organic synthesis method which gave us a good yield (Scheme 1). The process was easy, fast, decreased reaction time, and with no side reactions. The product is characterized and established by ^{1}H-NMR, ^{13}C-NMR, HR-MS analysis (Fig. S3-S5), and it was designed to chelate with metal ions via its carbonyl O and imine *N* atoms. The sensor **RD6g** consists of two units of rhodamine moieties and phenyl ring using hydrazide as the linker and coordination sites for Hg^{2+} ion.

Photophysical studies

The sensing ability of **RD6g** was investigated by ultraviolet/visible absorption spectroscopy. The compound did not show any absorption band above 400 nm, which is typical for the most prominent ring-closed spirolactone of rhodamine derivatives (Fig.S1). The changes in absorption spectra of **RD6g** with the supplement of various metal ions examined in acetonitrile–water (9:1; v/v) buffer system. The interaction studies performed with metal ions showed **RD6g** is very selective and sensitive towards Hg^{2+}. The sensor displays a characteristic peak of ring opened amide form of rhodamine at 530 nm with a shoulder at 490 nm (Fig. 1a). A new absorption band

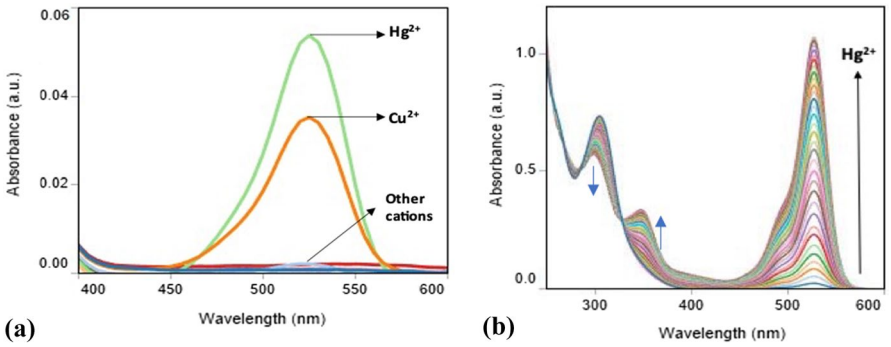

Fig. 1 **a** UV–Vis absorption spectra of **RD6g** (10 μM) with 20 μM various cations (Na^+, K^+, Mg^{2+}, Ca^{2+}, Ni^{2+}, Zn^{2+}, Co^{2+}, Hg^{2+}, Pb^{2+}, Cd^{2+}, Cu^{2+}, Fe^{2+}, and Fe^{3+}) in CH_3CN/H_2O (9:1 v/v) buffer system. **b** UV–Vis's absorption spectra of **RD6g** (3 μM) with Hg^{2+} (0–310 μM) in acetonitrile–water (9:1 v/v) buffer solution

Fig. 2 Colorimetric changes of **RD6g** (20 μM) upon the addition of 10 equiv. of various metal ions in CH_3CN/H_2O (9:1 v/v) at room temperature

produced at A_{530} nm, and isosbestic points at 280 and 330 nm, demonstrating that a metal complex was formed. The new absorption band gradually increases and saturated at 2.2 equivalent of Hg^{2+} ions (Fig. 1b). The change in color from colorless to pink demonstrated the opening of the spirolactam ring upon coordination with Hg^{2+} ions. The color change noted after the addition of all the metal ions tested was photographed and shown in Fig. 2. As shown in Fig. 3a, a Job's plot experiment was conducted. The maximum absorbance intensity at 530 nm was appeared with mole fraction of Hg^{2+} was close to 0.5, which indicated that 1:1 stoichiometry was the most possible binding mode of Hg^{2+} and **RD6g**. The association constant (K) between Hg^{2+} and **RD6g** was found to be 2.4×10^7 M^{-1} in CH_3CN/H_2O (9:1; v/v) buffer solution based on 1:1 stoichiometry.

Rhodamine derivatives have been described to develop fluorescent sensors for the identification of cations because of a ring-opening and structural change of a sensing compound. To evaluate the optimal conditions for the detection of metal ions, it is necessary to investigate the pH effect on fluorescence response of sensor **RD6g.** The sensor **RD6g** exhibits very strong fluorescence at the low

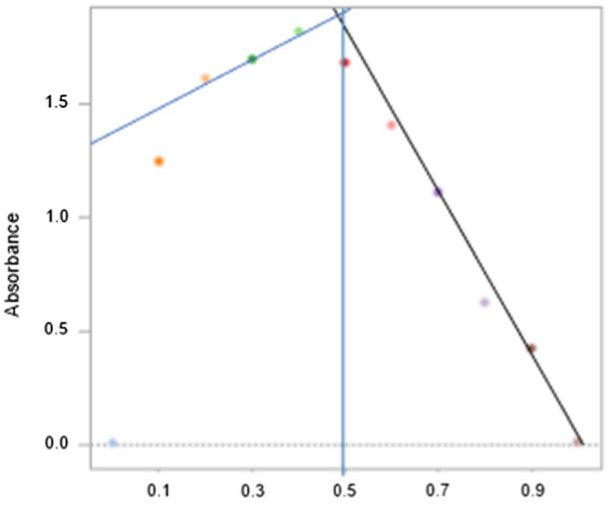

(a) [Hg^{2+}]/**RD6g**+Hg^{2}]

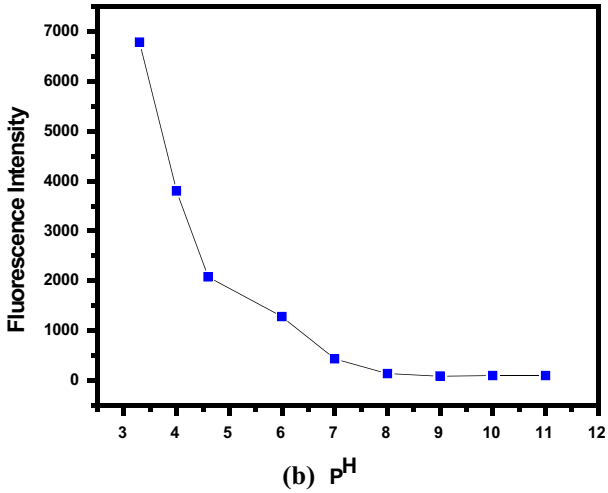

(b) P^{H}

Fig. 3 **a** Job's plot experiment of **RD6g** versus Hg^{2+} ([**RD6g**] + [Hg^{2+}] = 20 μM) in acetonitrile–water solution. **b** Effect of pH on fluorescence intensity of sensor **RD6g** (10 μM)

pH range (Fig. 3b). When pH>6.5, there are not obviously fluorescence intensity change, which may be caused by closed structure. Thus, all the optical measurements were conducted in acetonitrile–water (9:1, v/v, 10 mM Tris–HCl buffer, pH of 7) to maintain the ring-closed spirolactam form of the sensor. As expected, the free sensor **RD6g** exhibited very weak fluorescence above 520 nm (λ_{ex},510 nm) in the acetonitrile/water ((9:1); v/v) buffer system. The selectivity of this proposed sensor RD6g was conducted in acetonitrile–water, and the tested cations

used were Na^+, K^+, Mg^{2+}, Ca^{2+}, Ni^{2+}, Cu^{2+}, Cd^{2+}, Zn^{2+}, Co^{2+}, Hg^{2+}, Pb^{2+}, Fe^{2+}, Fe^{3+} (Fig. 4). The study revealed that the interaction of Hg^{2+} induced the fluorescent enhancement of **RD6g** at 560 nm (Fig. 4a). The fluorescence intensity change attributed with the formation of ring-opened spirolactam amide form of sensor **RD6g** upon binding with Hg^{2+} ion. The visual color change from colorless to light green examined under 365 nm light in darkness confirmed the formation of a fluorescent ring open form of spirolactam (Figure b, inset). The study also revealed the interaction with copper (II) ion. Like some other similar reported rhodamine-based Hg^{2+}sensors [31–35], the emission intensity of **RD6g** were also affected in the presence of paramagnetic copper (II) ion. Copper (II) may get involved in the coordination with **RD6g** and form a ring-opened system. In the fluorescence emission detection of Hg^{2+} using sensor **RD6g**, it is very important to avoid a high concentration of copper (II) ion interference using a quinoline-based derivatives [36]. Other tested cations did not have an influence on the fluorescence emission spectrum of the sensor **RD6g**. The incremental addition of Hg^{2+} to **RD6g** enhances fluorescence intensity at 560 nm and gets saturated at 20 equivalents of Hg^{2+} ion (Fig. 4b). The detection limit of **RD6g** for Hg^{2+} was estimated based on the fluorescence titration as 1.2×10^{-8} M.

The fluorescence lifetime measurement is used for investigating various properties of excited-state dynamics and molecular interactions. The fluorescence lifetime of the sensor **RD6g** with Hg^{2+} and Cu^{2+} was explored to confirmed photophysical studies of the sensor (Fig. 5). For the sensor **RD6g**, it was clear that the incorporation of the Hg^{2+} impacted the lifetime of the corresponding rhodamine derivative. The free sensor **RD6g**, [RD6g·Hg^{2+}], and Cu^{2+}complex displayed second exponential characteristics. The [RD6g·Hg^{2+}] complex showed the longest lifetime followed by the free **RD6g** and then **RD6g** with Cu^{2+} (Table S2). It is obvious that the addition of metal ions can affect the time a rhodamine derivative spends in the excited state before emitting a photon and returning to the ground table. The fluorescence emission and colorimetric sensing method toward Hg^{2+} was compared with some other described fluorescence emission sensing methods of Hg^{2+}, as listed in Table 1, [37–42].

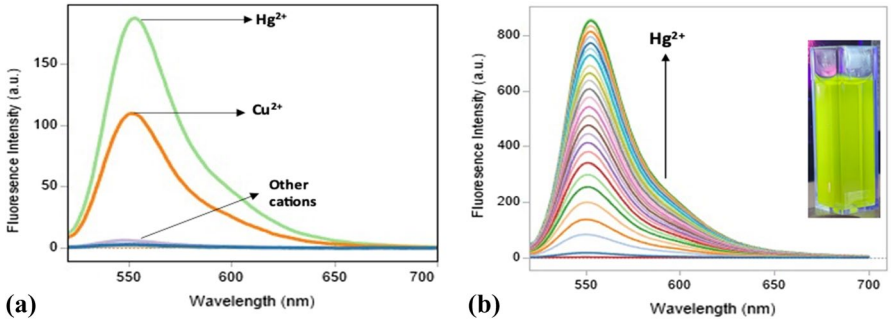

Fig. 4 **a** Fluorescence emission spectra of **RD6g** (20 μM) with metal ions in CH_3CN/H_2O (9:1 v/v) buffer solution (excitation wavelength, 510 nm). **b** Fluorescence emission spectra of **RD6g** (20 μM) with Hg^{2+} (0–20 μM) in CH_3CN/H_2O (9:1 v/v) solution

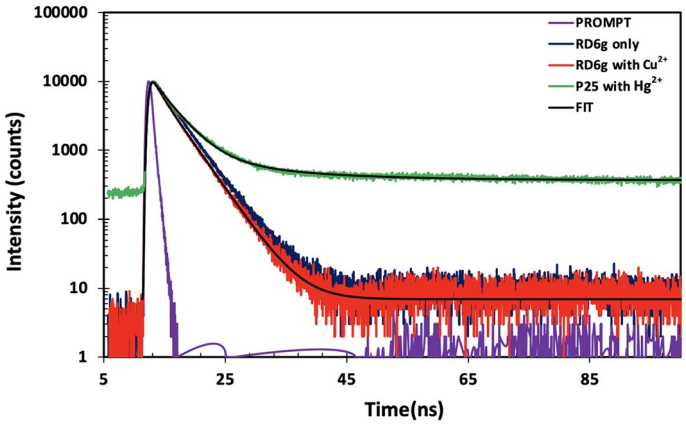

Fig. 5 Fluorescence lifetime measurements of **RD6g** and metal complexes

Coordination mechanism of RD6g with Hg^{2+}

The 1:1 stoichiometry between **RD6g** and Hg^{2+} is confirmed by Job's plot experiment. Likewise, the coordination between **RD6g** and Hg^{2+} ion is confirmed by the ^{1}H-NMR titration experiment in DMSO-d_6. Figure 6 comprises two distinct spectra, in which the bottom was recorded only for **RD6g** while the top spectra comprise **RD6g** with 1.0 equivalents of Hg^{2+}. The sensor **RD6g** bears a chemical shift at 5.06 ppm for the NH group, which completely disappeared in the addition of 1 equivalent of Hg^{2+} ion ([RD6g·Hg^{2+}]) complex. The disappearance of NH signal suggests that due to coordination of Hg^{2+}ion with **RD6g** delocalized xanthene tautomer of the rhodamine moiety is formed. The partial ^{1}H-NMR spectrum of **RD6g** shows the signal at δ 8.40 corresponds to N=CH proton which gets slightly shifted (δ 0.02) down filled with the addition of 1 equivalent of Hg^{2+} ion. The characteristic

Table 1 The comparison of **RD6g** with other reported colorimetric and fluorescent sensors

Sensing material	System	LOD	Real sample	References
Fluorescein	Dichloromethane	2.02×10^{-8} M		[34]
BODIPY	CH_3CN–H_2O (1:1v/v)	1.81×10^{-7} M	Test papers	[35]
Pyrene	HEPES–CH_3CN (3:7v/v)	36 nM	Test strips and silica gel pates	[36]
Naphthalimide	DMSO–H_2O (1:99v/v)	14.7 nM	Water samples	[37]
Sensor L2	H_2O (P^H 7.4)	6.09×10^{-8} M	HeLa cells	[38]
Tetraphenyl	C_2H_5OH–H_2O (3:5)	45.4 nM	Tap water	[39]
Coumarin	CH_3CN–H_2O (3:2v/v)	5×10^{-8} M	Filter paper	[40]
Indole	HEPES	1.08 μM	HeLa cells	[41]
Rhodamine B	CH_3CN–HEPE 1:99v/v	0.14 μM		[42]
Rhodamine6G	CH_3CN–H2O (9:1v/v)	1.2×10^{-8} M		This work

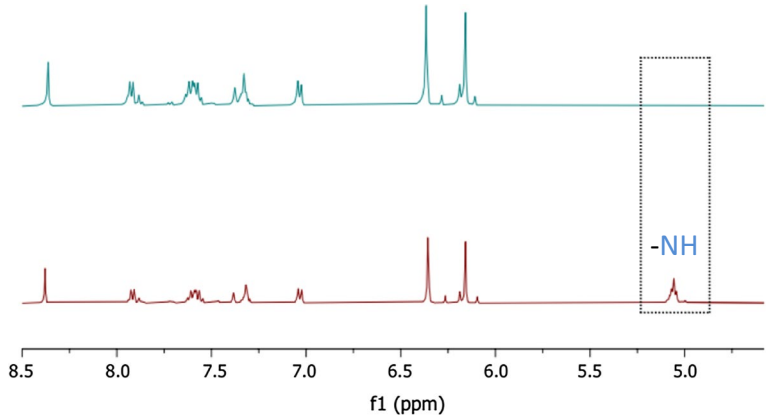

Fig. 6 Partial ^{1}H-NMR spectra of **RD6g** in the absence and presence of 1 equivalent of Hg $(NO_3)_2$ salt in DMSO-d_6

carbonyl stretching frequency at 1720 cm^{-1}in the IR spectra also slightly shifted to 1718 cm^{-1} and the intensity of the peak decreased upon coordination with Hg^{2+}(Fig. S6). As a result of the above description, **RD6g** is most likely to coordinate with Hg^{2+} via oxygen on the carbonyl group and nitrogen on the hydrazine group. The plausible binding mode of **RD6g** toward Hg^{2+} is shown in Scheme 2.

Cyanide detection

Further, it was of great interest to investigate the reversible binding nature of the sensor **RD6g**. Figure 7a shows the addition of 20 μM of anions to [RD6g·Hg^{2+}] (1:1) complex of which CN^- changes the emission band at 560 nm. Other common anions (Cl^-, I^-, F^-, ClO_4^-, CH_3COO^-, HSO_4^-, PO_4^{3-}, SCN^-, and OH^-) did not generate the same results. It indicated that CN^- can peel Hg^{2+} from the coordination region and sensor **RD6g** is reversible. The process was found to be resulting in a net color change from pink to colorless, which was observed with the naked eye. The absorption profile of **RD6g** with anions was very similar to the fluorescence emission spectra: again CN^{-1} ion changes the absorption intensity while other anions showed no significant change (Figure S2). Due to the stability of $Hg(CN)_2$, the [RD6g·Hg^{2+}] complex could be used as a possible means to detect CN^- ion. The

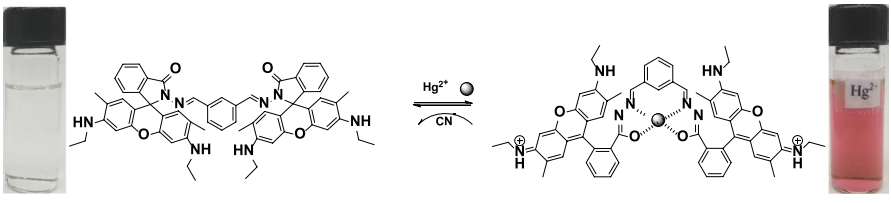

Scheme 2 Proposed reversible 1:1 binding mode of **RD6g** and Hg^{2+}

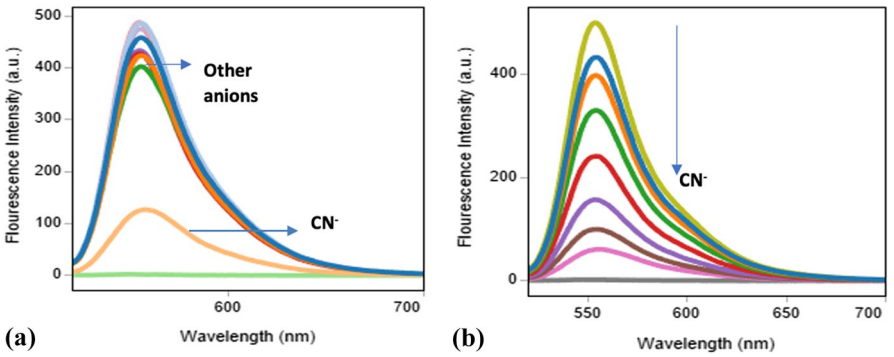

Fig. 7 **a** Fluorescence spectra of [RD6g·Hg^{2+}] complex in presence of anions (Cl^-, I^-, CN^-, F^-, ClO_4^-, CH_3COO^-, HSO_4^-, PO_4^{3-}, SCN^-, and OH^-) **b** Fluorescence spectra of [RD6g·Hg^{2+}] complex upon addition of CN^- (0–5 equiv) in acetonitrile–water (9:1 v/v) solution

response mechanism between the sensor **RD6g** and Hg^{2+} in the presence of CN^- is shown in Scheme 2.

Filter paper test strip application

To explore the practical application of fluorescent sensor **RD6g**, test strips were prepared followed by the report procedure [43]. Sensor test strips were fabricated by immersing Whatman filter paper into acetonitrile solution of **RD6g** (1 mM) for one minute and the test strips were air-dried before use. Then, these test strips holding **RD6g** were used to detect Hg^{2+}. As shown in Fig. 8, an obvious color change, colorless to green, was observed under the 365 nm UV lamp which confirms the presence of Hg^{2+}. Other potential competitive metal ions did not produce any color changes on the test strips. The significant quenching of fluorescence and disappearance of greenish color in the RD6g + Hg^2 system due to regeneration of **RD6g** was observed in the presence of CN^- ions. It suggests that the strong interaction of Hg^{2+} and CN^- ions possibly facilitates the rapture of the RD6g. Hg^{2+} complex in support of a quenching phenomenon. The results demonstrate that the obtained RD6g.Hg^{2+} complex can be used as an efficient fluorescent sensor for recognition CN^-. Therefore, this study indicated that filter paper test strips of **RD6g** could easily sense both Hg^{2+} and CN^- colorimetrially and fluorometrically in solid state.

Time-dependent density functional theory (TD-DFT) studies

Time-dependent density functional theory (TD-DFT) calculations were employed to elucidate Hg^{+2} interactions with the **RD6g** system. All computations were carried out using the Spartan '18 software package. Employing the Spartan '18 (TDA) B3LYP functional and the 6-31G(d,p) basis set, sensor **RD6g** and its respective [RD6g·Hg^{2+}] complex was optimized in the gas phase (vacuum), and in both simulated CH_3CN and water media, using a conductor-like polarizable

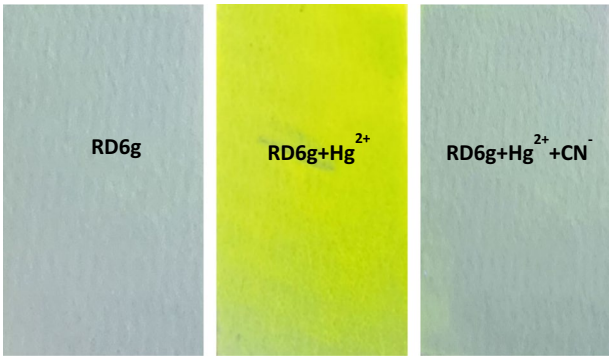

Fig. 8 (Color online) Photographs of colorimetric test strips with **RD6g** for sensing Hg^{2+} and CN^{-} simultaneously under irradiation at 365 nm

continuum model (CPCM). Vertical electronic absorption and fluorescence emission data of the said optimized structures were obtained and compared with empirical obtained UV–Vis data. Wavelengths and oscillator strengths (*f*) for prominent vertical electronic excitations, as well as emission data for both sensor and complex, are highlighted.

For sensor **RD6g** in the gas phase, the energy gap between the highest occupied molecular orbital (HOMO = − 5.06 eV) and the lowest unoccupied molecular orbital (LUMO = − 1.04 eV) is 4.02 eV. Four computed, prominent vertical electronic transitions are highlighted for **RD6g** with wavelengths and f values as follows: 271.70 nm (f = 0.1515), 280.85 nm (f = 0.1216), 296.98 nm (f = 0.1775) and 308.15 nm (f = 0.1170). Upon formation of gaseous [RD6g·Hg^{2+}] complex from RD6g and Hg^{+2}, the frontier energy gap decreased from 4.02 to 1.26 eV, [RD6g·Hg^{2+}], HOMO = − 8.99 eV, and LUMO = − 7.73 eV). And the four computed, prominent electronic transitions for [RD6g·Hg^{2+}] complex in vacuum are at: 476.57 nm (f = 0.0418), 526.52 nm (f = 0.0198), 683.02 nm (f = 0.0220), and 1178.95 nm (f = 0.1506). For sensor **RD6g** in CH_3CN, the frontier energy gap is much smaller than in vacuum, ΔE = 3.60 eV (**RD6g** in CH_3CN, HOMO = − 5.28 eV and LUMO = − 1.68 eV) as opposed to 4.02 eV. The four prominent transitions for **RD6g** in CH_3CN are at 294.52 nm (f = 0.4369), 310.29 nm (f = 0.1855), 318.20 nm (0.8064), and 334.48 nm (f = 0.2809). On forming [RD6g·Hg^{2+}] complex from **RD6g** and Hg^{+2} in CH_3CN, ΔE (**RD6g**) changed from 3.60 to 2.47 eV (CH_3CN), and the four prominent transitions for [RD6g·Hg^{2+}] complex in CH_3CN are at 339.81 nm (f = 0.2249), 405.75 nm (f = 0.1105), 597.25 nm (f = 0.0449) and 605.03 nm (f = 0.0318). For sensor **RD6g** in water, the frontier energy gap (ΔE) is = 3.58 eV (HOMO = -5.28 eV and LUMO = − 1.70 eV), which is slightly less than in CH_3CN, ΔE = − 3.60 eV. The four prominent transitions for **RD6g** in water are at 285.36 nm (f = 0.1812), 288.89 nm (f = 0.2487), 305.89 nm (0.1826), and 314.43 nm (f = 0.7889). For [RD6g·Hg^{2+}] in water, ΔE is slightly larger (2.49 eV, HOMO = − 5.44 eV and LUMO = − 2.95 eV) than in CH_3CN, ΔE = 2.47 eV. The four computed,

prominent electronic transitions for [RD6g·Hg^{2+}] in water are at 337.99 nm (f = 0.1860), 402.94 nm (f = 0.0954), 487.73 nm (f = 0.0276), and 589.72 nm (f = 0.0447).

In the gas phase, HOMO of **RD6g** is found primarily centered on one of the xanthene moieties (Fig. 9), whereas, in both acetonitrile and water (Figs. 10 and 11), HOMO is found throughout both xanthene moieties. In all three media, LUMO of **RD6g** is found about the spirolactam moiety, including the two imine groups and the carbonyl oxygens but is absent about the ethereal oxygens and part of the connecting phenyl group. However, in these same three media, HOMO of [RD6g·Hg^{2+}] complex appears to be delocalized over the same position in the two xanthene moieties. And LUMO is found exclusively about the region connecting the two xanthene moieties which include Hg^{+2}, the two carbonyl oxygens, the two imine groups, and part of the phenyl group.

In the gas phase, sensor **RD6g** is described by three computed, prominent emission wavelengths, one at 360.72 nm (f = 0.2102), a second at 373.17 (f = 0.2792) and a third at 380.51 nm (f = 0.4213); [RD6g·Hg^{2+}] complex in vacuum is also described by three prominent ones as well: 1061.23 (f = 0.0111), 1178.94 (f = 0.1503) and 1388.50 (f = 0.0184). In CH_3CN, sensor **RD6g** is described by three prominent emission wavelengths at: 392.06 nm (f = 0.0031), 393.50 nm (f = 0.0841) and 410.03 (f = 0070). For [RD6g·Hg^{2+}] complex in CH_3CN, three computed, prominent emission wavelengths are at: 491.57 nm (f = 0.0317), 597.25 nm (f = 0.0450), and 605.03 nm (f = 0.0315). And for sensor **RD6g** in water, the three prominent emission transitions computed are at: 406.79 nm (f = 0.0153), 407.35 nm (f = 0.0178), and 423.91 nm (f = 0.0614), and

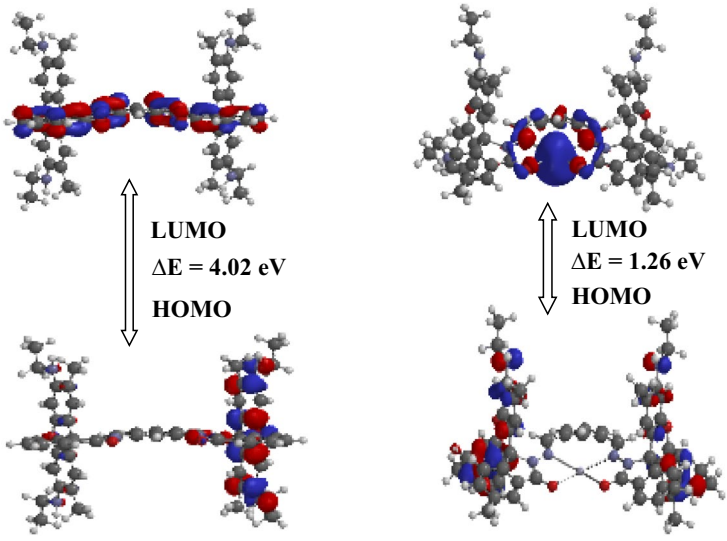

Fig. 9 Optimized Structures and Frontier Molecular Orbitals of **RD6g** and bis-(**RD6g**)$_2Hg^{+2}$ complex in the Gas Phase

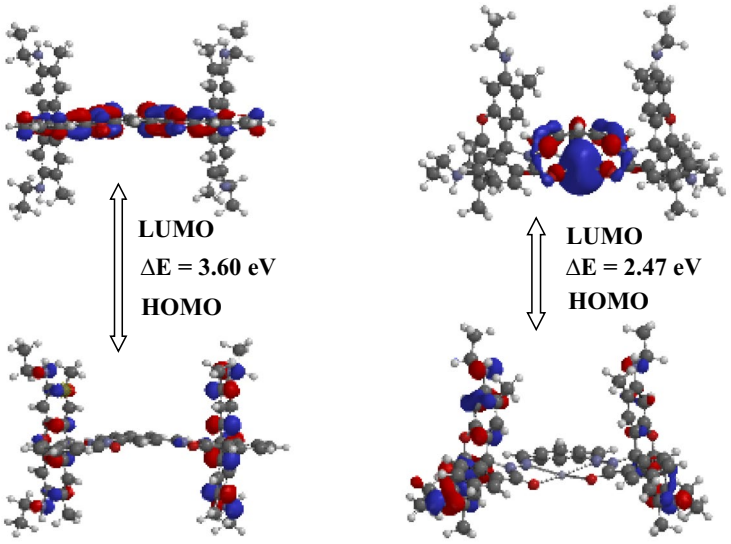

Fig. 10 Optimized Structures and Frontier Molecular Orbitals of **RD6g** and [RD6g·Hg^{2+}] complex in simulated CH_3CN medium

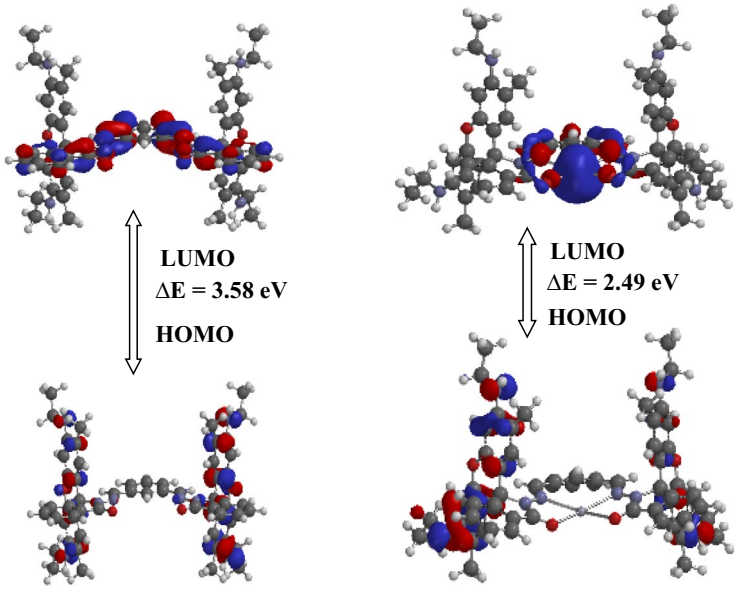

Fig. 11 Optimized Structures and Frontier Molecular Orbitals of **RD6g** and [RD6g·Hg^{2+}] complex in simulated water medium

for [RD6g·Hg^{2+}] complex in water, the three prominent emission transitions are at: 487.43 nm ($f = 0.0274$), 589.25 nm ($f = 0.0449$), and 596.76 nm ($f = 0.0204$).

Conclusion

In conclusion, a simple rhodamine-based colorimetric and fluorescent sensor **RD6g** for the detection of Hg^{2+} ions has been synthesized using microwave irradiation. The sensor **RD6g** displayed a highly sensitive fluorescence increment upon the addition of an Hg^{2+} ion. Clear visible color change from colorless to pink allows **RD6g** to use as a naked eye sensor. The stoichiometry of the 1:1 complex was recognized for a mole fraction of 0.5. Moreover, the detection limit of the sensor **RD6g** for Hg^{2+} was 1.2×10^{-8} M, which indicated that the sensor could be useful as a highly selective and sensitive sensor for detecting Hg^{2+}. Further, the reversible switch of complex [RD6g·Hg^{2+}] was investigated and attained in the presence of a CN^{-1} ion. The test strip based on **RD6g** was developed, which could be used as a suitable and methodical Hg^{2+} test kit. The design of bis(rhodamine)-based compounds can be further explored to obtain highly selective and sensitive sensors.

Supplementary Information The online version contains supplementary material available at https://doi.org/10.1007/s11164-022-04704-x.

Acknowledgements This work was supported by the National Science Foundation's Division of Chemistry under Grant [2100629] and Morgan State University.

Declarations

Conflict of interest No potential conflict of interest was reported by the authors.

References

1. J. Gutknecht, J. Membr. Biol. **61**, 61–66 (1981)
2. D. Camur, C. Gueler, S.C. Vaizoglu, Toxicol. Ind. Health **32**, 1215–1223 (2016)
3. L.L. Tan, Y. Zhang, H. Qiang, Sens. Actuators B: Chem. **229**, 686–691 (2016)
4. X. Zhu, Y. Yuan, L. Li, Mater. Des. **A29**, 91–102 (2017)
5. D. Sun, G. Sun, X. Zhu, Fuel **211**, 609–620 (2018)
6. Y. Yang, S. Rong, W. Ying-Zhe, Sens. Actuator B: Chem. **255**, 3479–3487 (2018)
7. Z. Sun, M. Yang, Y. Ma, I. Li, Cryst. Growth Des. **17**, 4326–4335 (2017)
8. F.X. Han, W.D. Patterson, Y.J. Xia, B.B. Sridhar, Y. Su, Water Air Soil Pollut. **170**, 161–171 (2006)
9. T. Li, S.J. Dong, E. Wang, Anal. Chem. **81**, 2144–2149 (2009)
10. M.H. Mashhadizadeh, I. Sheikhshoaie, Talanta **60**, 73–80 (2003)
11. E.C. Rupp, E.J. Granite, D.C. Stanko, Anal. Chem. **82**, 6315–6317 (2010)
12. Z. Yang, S. Chen, Y. Zhao, P. Zhou, Z. Cheng, Sens. Actuators B **266**, 422–428 (2018)
13. W. Huang, X. Zhu, D. Wua, C. He, X. Hu, C. Duan, Dalton Trans. **45**, 10457–10465 (2009)
14. Q. Wang, L. Jin, W. Wang, T. Hu, C. Chen, J. Lumin. **209**, 411–419 (2019)
15. G. Heo, D. Lee, C.G. Kim, J.Y. Do, Spectrochim. Acta Part A Mol. Biomol. Spectrosc. **188**, 285–290 (2018)
16. F. Abebe, P. Perkins, R. Shaw, S. Tadesse, J. Mol. Struct. **1205**, 127594 (2020)
17. F. Abebe, T. Sutton, P. Perkins, R. Shaw, Luminescence **33**, 1194–1201 (2018)
18. F. Abebe, J. Gonzalez, K. Makins-Dennis, R. Shaw, Inorg. Chem. Commun. **120**, 108154 (2020)

19. M. Desi, H. Basu, S. Saha, R. Singhal, S. Kailasa, J. Mol. Liq. **336**, 116239 (2021)
20. M. Kateshiya, G. George, J. Rohit, N. Malek, S. Kailasa, Microchem. J. **158**, 105212 (2020)
21. S.K. Patil, D. Das, Spectrochim. Acta A. Mol. Biomol. Spectrosc. **210**, 44–51 (2019)
22. P.G. Rao, B. Saritha, R.T. Siva, J. Fluoresc. **29**, 353–360 (2019)
23. K. Zhang, J. Zhang, Res. Chem. Intermed. **46**, 987–997 (2020)
24. C. Wang, L. Wang, S. Fang, D. Quin, J. Zhou, G. Yang, S. Jin, H. Duan, Res. Chem. Intermed. **45**, 2045–2063 (2019)
25. J.H. Hu, C. Long, Q.Q. Fu, P.W. Ni, Z.Y. Yin, J. Photochem. Photobiol. A Chem. **379**, 105–111 (2019)
26. R. Ji, A. Liu, S. Shen, X. Cao, F. Li, Y. Ge, RSC Adv. **7**, 40829–40829 (2017)
27. Y. Fang, Y. Zhou, J.Y. Li, Q.Q. Rui, C. Yao, Sens. Actuators B Chem. **215**, 350–359 (2015)
28. K. Song, J. Mo, C. Lu, Spectrochim. Acta A. Mol. Biomol. Spectrosc. **179**, 125–334 (2017)
29. H. Jiqu, Y. Qixia, Spectrochim. Acta A. Mol. Biomol. Spectrosc. **149**, 487–493 (2015)
30. A. Leite, A. Silva, L. Cunha-Silvs, B. Castro, P. Gameiro, M. Rangel, Dalton Trans. **42**, 6110–6118 (2013)
31. G. Li, L. Bai, F. Tao, A. Deng, L. Wang, Analyst **143**, 5395–5403 (2018)
32. H.Y. Lee, K.M.K. Swamy, J.Y. Jung, G. Kim, J. Yoon, Sens. Actuators B **182**, 530–537 (2013)
33. S. Shyamsivappan, A. Saravanan, N. Vandana, T. Surash, S. Surash, R. Nandhakumar, P. Mohan, ACS Omega **42**, 27245–27253 (2020)
34. N. Wanichacheva, O. Hanmeng, S. Kraithong, K. Sukrat, J. Photochem. Photobiol. A Chem. **278**, 75–81 (2014)
35. A. Maity, A. Sil, S. Nad, S.K. Patra, Sens. Actuators B **255**, 299–308 (2018)
36. C.B. Bai, P. Xu, J. Zhang, R. Qiao, M.Y. Chen, M.Y. Mei, B. Wei, C. Wang, L. Zhang, S.S. Chen, ACS Omega **4**, 14621–14625 (2019)
37. M. Bahta, N. Ahmed, J. Photochem. Photobiol. A Chem. **391**, 112354 (2020)
38. A. Kumar, R. Ananthakrishnan, G. Jana, P. Pratim, P.K. Chattaraj, S. Nayak, S.K. Ghosh, ChemistrySelect **4**, 4810–4819 (2019)
39. Y. Yuan, X. Chen, Q. Chen, G. Jiang, H. Wang, J. Wang, Anal. Biochem. **585**, 113403 (2019)
40. A. Shaily, N. Kumar, Ahmed. Ing. Eng. Chem. Res. **56**, 6358–6368 (2017)
41. Y. Zhang, C. Zhang, Y. Wu, B. Zhao, L. Wang, B. Song, RCS Adv. **9**, 23382–23389 (2019)
42. M. Hong, Y. Chen, Y. Zhang, D. Xu, Analyst **144**, 7351–7358 (2019)
43. R. Qiao, W.Z. Xiong, C.B. Bai, J.X. Liao, L. Ahang, Supramol. Chem. **30**, 911–917 (2018)